Appl. Phys. A 75, 237–246 (2002)
DOI: 10.1007/s003390201335

Applied Physics A
Materials Science & Processing

Quantum ratchets and quantum heat pumps

H. LINKE[1,✉]
T.E. HUMPHREY[2]
P.E. LINDELOF[3]
A. LÖFGREN[4]
R. NEWBURY[2]
P. OMLING[4]
A.O. SUSHKOV[2]
R.P. TAYLOR[1]
H. XU[4]

[1] Department of Physics, University of Oregon, Eugene, OR 97403-1274, USA
[2] School of Physics, University of New South Wales, Sydney 2052, Australia
[3] Niels-Bohr-Institute, University of Copenhagen, Universitetsparken 5, 2100 Copenhagen, Denmark
[4] Solid State Physics, Lund University, Box 118, 22100 Lund, Sweden

Received: 8 February 2002/Accepted: 11 February 2002
Published online: 22 April 2002 •

ABSTRACT Quantum ratchets are Brownian motors in which the quantum dynamics of particles induces qualitatively new behavior. We review a series of experiments in which asymmetric semiconductor devices of sub-micron dimensions are used to study quantum ratchets for electrons. In rocked *quantum-dot ratchets* electron-wave interference is used to create a non-linear voltage response, leading to a ratchet effect. The direction of the net ratchet current in this type of device can be sensitively controlled by changing one of the following experimental variables: a small external magnetic field, the amplitude of the rocking force, or the Fermi energy. We also describe a tunneling ratchet in which the current direction depends on temperature. In our discussion of the tunneling ratchet we distinguish between three contributions to the non-linear current–voltage characteristics that lead to the ratchet effect: thermal excitation over energy barriers, tunneling through barriers, and wave reflection from barriers. Finally, we discuss the operation of adiabatically rocked tunneling ratchets as *heat pumps*.

PACS 73.40.Ei; 73.23.Ad; 73.50.Fq; 7.20.Pe

1 Introduction

Quantum ratchets are Brownian motors [1] in which the particles' quantum behavior, such as wave interference, or the tunneling into classically forbidden areas leads to a significantly modified particle current compared to the classical behavior. The concept of quantum ratchets was first conceived by Reimann, Grifoni and Hänggi [2], who numerically studied the quantum-mechanical counterpart of the classical, adiabatic rocking ratchet. A rocking ratchet is an asymmetric potential that is symmetrically tilted or "rocked" by an external force which is zero on average over time (Fig. 1) [3]. The expression "adiabatic" refers to a rocking time scale that is longer than any characteristic time of the system, such that the system is in a steady state at each instant in time. In the present contribution we review a series of experiments in which quantum behavior in ratchets was observed for the first time.

Our experimental system is the so-called "mesoscopic" semiconductor device, in which electron transport effects can be studied in a regime that lies between "large", macroscopic systems, where classical, ohmic behavior is observed, and extremely small, fully quantum-mechanical systems, such as atoms. The mesoscopic regime of electron transport is illustrated in Fig. 2, in which Fig. 2a is a top-view scanning electron micrograph of an electron cavity. The darker areas in the image are trenches patterned by electron beam lithography and subsequent wet-etching. These trenches serve to interrupt a sheet of electrons located at the interface of a GaAs/AlGaAs heterostructure, typically 30–100 nm below the surface. This sheet forms a so-called two-dimensional electron gas (2DEG) – electrons can move within the plane of the image, but electrostatic confinement restricts motion in the third dimension. The etched trenches electrically isolate the inner part of the triangle – the electron cavity – from the surrounding 2DEG areas, except for two narrow openings (so-called point contacts), visible at the tip and in the center of the base of the triangle. The dimension of the cavity is typically of the order of a micrometer, which at low temperatures ($T < 10$ K) is much smaller than the characteristic length scales for electron scattering. In this so-called ballistic limit, the dynamics of electrons is well-described by a single-particle picture, in which electrons move along straight trajectories between boundary collisions [4, 5] (Fig. 2b). Because of the similarity with a game of billiards, ballistic two-dimensional cavities are often referred to as electron billiards.

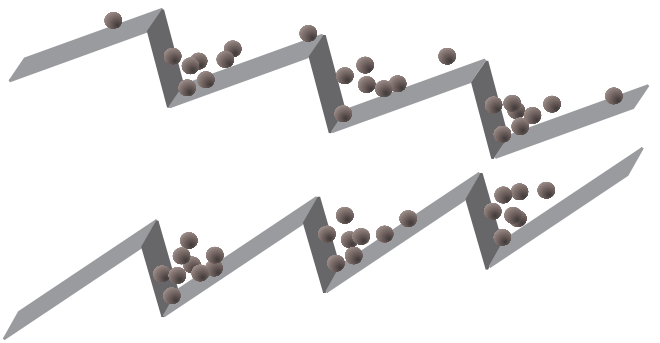

FIGURE 1 A rocking ratchet is an asymmetric potential that is periodically or randomly tilted such that the time-averaged tilt is zero. The net (time-averaged) particle current is qualitatively different when quantum effects such as tunneling are taken into account (see text)

Three length scales are important for the observation of quantum effects in electron billiards: (i) the *phase coher-*

✉ Fax: +1-541/346-5861, E-mail: linke@darkwing.uoregon.edu

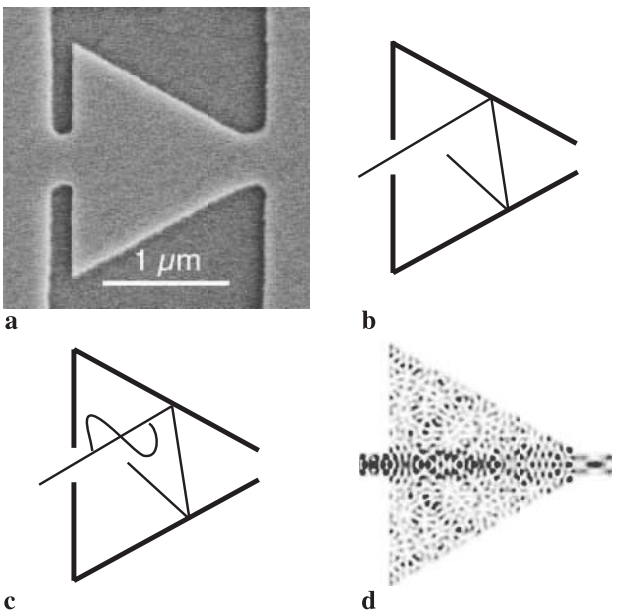

FIGURE 2 **a** Scanning-electron micrograph of a triangular electron cavity (top view). The *darker areas* are wet-etched trenches that electrically interrupt a sheet of electrons located about 100 nm below the surface. **b** At low temperatures electrons move along straight trajectories between collisions with the boundaries, similar to a game of billiards. **c** When electron transport is phase coherent, a semiclassical description of transport is useful. In this picture electrons move along classical trajectories and are equipped with a phase. **d** In a fully quantum-mechanical description the Schrödinger equation is solved and electron quantum states are calculated (calculation by Igor Zozoulenko in [14])

ence length, l_ϕ; (ii) the *electron wavelength* at the Fermi energy, λ_F; and (iii) the *characteristic length* for tunneling effects. l_ϕ is the length scale over which the wave character of electrons (the phase memory) is preserved and where wave-interference effects can be observed [4, 5]. l_ϕ is limited by inelastic scattering events, such as electron–electron or electron–phonon interaction where the electron gains or loses energy. (It is important to note that elastic scattering, in particular the interaction of electrons with the billiard walls, does not destroy phase coherence.) l_ϕ can exceed tens of micrometers at sub-Kelvin temperatures, but it decreases quickly with temperature and is typically less than a micrometer at about 5 K. Wave-interference effects in a device as shown in Fig. 2a can therefore be switched on and off experimentally by tuning the temperature around 1 K – a very useful experimental tool that we will make use of in Sect. 2. The electron wavelength is the critical length scale for the observation of effects related to energy quantisation by spatial confinement. Quantisation effects are observable, for instance, in the conductance of the point contacts of the cavity in Fig. 2a. An electron can access a narrow constriction only when it's energy exceeds the lateral confinement energy $\hbar^2 k_y^2/2m^*$, where $k_y = 2\pi/\lambda_F$ is the component of the wave vector perpendicular (y direction) to the confining walls and m^* is the effective electron mass in the crystal [4, 5]. In a typical 2DEG the wavelength of electrons at the Fermi energy, λ_F, is about 40 nm, and quantisation effects can be observed for W of the order of 100 nm and less. When $W < \lambda_F/2$, transport through a point contact is at low temperatures not possible except by tunnelling. The length scale over which tunneling effects are appreciable (and measurable) is typically 10–100 nm.

The construction of a quantum ratchet requires: (i) particles subject to quantum effects; (ii) a controlled (a)symmetry of the rocked potential sensed by the particles; (iii) absence of detailed balance; and (iv) sensitivity to noise, such as thermal noise. With these requirements and the above discussion of relevant length scales in mind, consider now the device shown in Fig. 2. At sub-Kelvin temperatures electron transport across a device of this size is phase coherent. One can therefore switch from a classical, single-particle picture of the electron dynamics (Fig. 2b) to a semi-classical picture (where electrons have a phase but move on classical trajectories, Fig. 2c) or even to a fully quantum mechanical description (Fig. 2d). Quantum effects, such as interference of electrons (Fig. 2c), tunneling effects, and conductance quantisation lead to significant modifications of electron transport properties compared to macroscopic devices [4, 5], in fulfillment of (i). Because electron transport is ballistic, and because in the coherent transport regime the electron wave function extends throughout the cavity, the electron dynamics in electron billiards is determined by the shape and symmetry of the cavity. This gives us control over the symmetry of the potential experienced by the electrons. (In a macroscopic device with dimensions much larger than the electron mean free path, the symmetry of the overall device shape is unimportant for electron transport.) Finally, because of their small size, mesoscopic electron devices can easily be driven away from thermal equilibrium, breaking detailed balance [6], and quantum transport effects are extremely sensitive to thermal noise. Our experimental system thus fulfills all necessary requirements for the study of quantum ratchets.

Here we will review two specific experiments. In Sect. 2 we describe *quantum-dot ratchets* which use the sensitive response of electron-wave interference to an external electric field to partially rectify an ac voltage [7]. The rectification mechanism that is at work in the quantum-dot ratchet is distinct from that in a *tunneling ratchet*, discussed in Sect. 3, in which the non-linear response of a tunneling barrier is used to rectify a voltage. In this device, thermal noise can change the occupation of electron states in such a way that tuning the temperature reverses the net ratchet current [8]. To explain this observation, we will distinguish three different mechanisms for current generation, namely classical thermal excitation, tunneling, and the electron wave reflection occurring at a potential step. In Sect. 4, we will briefly discuss how tunneling ratchets in which the current direction depends on temperature can also be analyzed in terms of a heat pump or heat engine [9, 10].

2 Quantum-dot ratchets

In the low-voltage, linear response regime of electron transport, the device conductance, $G = I/V$, is independent of the voltage, V, and electric conduction is symmetric by definition. The adiabatic operation of a rocking ratchet (Fig. 1) requires rectification – that is, a finite net current, $I_{net} = (1/2)[I(V) + I(-V)]$. Rectification is represented by the lowest order of non-linearity in the expansion $I(V) = G_0 V + G_1 V^2 + G_2 V^3 \ldots$ of the current. G_1 can be

non-zero in systems that lack a symmetry axis with respect to the current direction. Different types of rocking ratchets are distinguished by the way non-linear effects are induced. Mesoscopic devices are very easily driven into non-linear response [6] because transport via electron quantum states is very sensitive to external perturbations. In the following we will review basic properties of electron transport in mesoscopic devices (Sect. 2.1), before describing experimental results in Sect. 2.2.

2.1 *Basics: Conductance fluctuations in quantum dots*

To describe electron transport through a device as shown in Fig. 2, the two point contacts are usually viewed as the ends of a one-dimensional (1D) wave guide connected to source and drain electron reservoirs. The electron cavity is represented as a scattering potential, $U(V)$, with energy-dependent transmission probability, $t(\varepsilon, U(V))$. The current flowing between reservoirs is then given by the product of the conductance of the 1D wave modes ($2e/h$ per fully occupied wave mode) and $t(\varepsilon, U(V))$. It can be written as follows [5, 11]:

$$I(V) = \frac{2e}{h} \int t\,(\varepsilon, U(V))\, M(\varepsilon, V)\, [f_S(\varepsilon) - f_D(\varepsilon)]\, \mathrm{d}\varepsilon \qquad (1)$$

where $M(\varepsilon, V)$ is a step function describing the integer number of 1D wave modes available for transport at each energy, ε. The equilibrium Fermi distribution functions, f_S and f_D, describe the occupation of energy levels in the source- and drain-electron reservoirs, respectively, with electrochemical potentials, μ_S and μ_D, where $\mu_S = (\mu_D + eV)$, and $e = -1.6 \times 10^{-19}$ C is the charge on an electron [12]. The bracket $[f_S - f_D]$ is the Fermi window and represents the energy range over which net-electron flow takes place [5]. The width of the Fermi window, about $(4kT + |eV|)$, is determined by the applied voltage, V, and the temperature smearing of the Fermi distribution functions.

In an experiment one applies a small current bias between the electron reservoirs and measures the voltage drop over the device to compute the conductance. It is useful to measure the conductance as a function of a perturbation, often a magnetic field, B, applied perpendicular to the plane of the 2DEG. Classically, the magnetic field causes the electrons to move along cyclotron orbits (illustrated in the inset to Fig. 3) with radius $r = m^* v_F / eB$ where v_F is the electron velocity at the Fermi energy [4]. Due to this perturbation, $t(\varepsilon, U(V))$ varies on a characteristic magnetic field scale, B_C, the field at which the cyclotron diameter equals the side length of the equilateral triangle (for the device used in Fig. 3, $B_C \approx 50$ mT). The experimental data represented as a dashed line in Fig. 3a were taken at a temperature of $T = 4.5$ K, sufficiently cold to be in the ballistic regime where undisturbed trajectories such as the one shown in Fig. 3 are possible. At this temperature the data lend themselves to a classical interpretation, and the global maximum of the resistance around $B = B_C$ in Fig. 3 can be related to the high probability of backscattering of trajectories similar to the one indicated in the inset [13].

Phase coherence can be "switched on" experimentally by lowering the electron temperature below $T \approx 1$ K. Inelastic electron–electron interaction, known to destroy electron wave coherence, is then suppressed, and the edge of the Fermi distribution is sharp enough to resolve effects related to energy quantisation. The solid line in Fig. 3 shows magnetoresistance data taken at $T = 0.3$ K [14]. Superimposed on the classical behaviour (dashed line) we observe rapid fluctuations on a magnetic field scale of a few mT and less, much smaller than the scale for classical behavior, $B_C \approx 50$ mT. While these magneto-conductance fluctuations appear noise-like, they are in fact highly reproducible in subsequent sweeps of B and are also perfectly symmetric in the direction of the magnetic field.

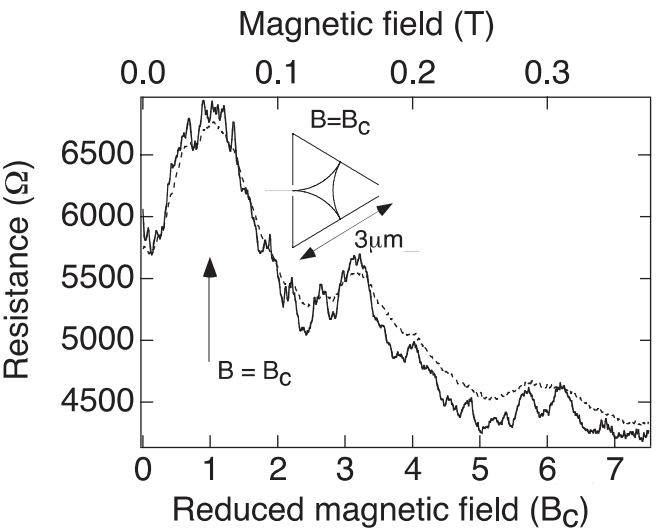

FIGURE 3 The electrical resistance of a triangular cavity (Fig. 2a) measured as a function of a magnetic field. The field is applied perpendicular to the cavity and causes the electrons to move along circular cyclotron orbits (see *inset*). At a few Kelvin (*dashed line*, $T = 4.5$ K) one can understand the main features of the resistance in terms of classical single-particles trajectories. In the phase-coherent regime (*solid line*, $T = 0.3$ K) electron interference establishes itself as conductance fluctuations superimposed on the classical behavior. (From [14])

The origin of magneto-conductance fluctuations can be explained in a semi-classical picture of electron transport in which a quantum-mechanical phase is added to the classical electron trajectories (Fig. 2c). Electron waves traveling along pairs of classical electron paths can interfere constructively or destructively. Using the Bohr–Sommerfeld quantisation condition, it is possible to identify short, periodic electron orbits with zero-dimensional (0D) electron states [15]. Transport of electrons through the billiard can then be viewed as a two-step process, in which electrons tunnel through one point contact onto a semi-classical electron state close to the Fermi energy and then leave this state through the second point contact (Fig. 4a). The conductance of the billiard is proportional to the number of states available at the Fermi energy inside the cavity. An external magnetic field shifts the electron phase and changes the interference. In particular, an electron state related to a specific closed orbit will be periodically "switched on and off" as the magnetic field is tuned, with period $\Delta B = h/eA$, given by the ratio of the orbit area, A, and the magnetic flux quantum, h/e. Consequently, the transmission probability, $t(\varepsilon)$, oscillates as a function of B with frequency spectrum components ΔB given by the areas of the contributing periodic orbits [16].

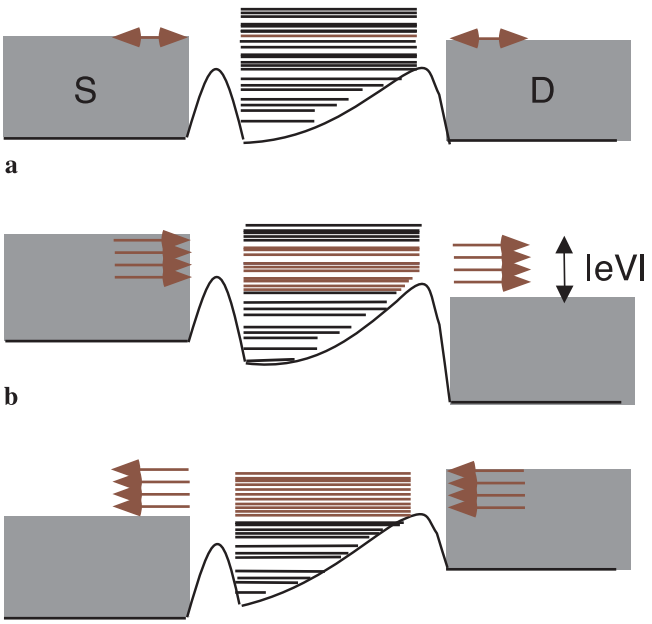

FIGURE 4 Illustration of electron transport through a quantum dot. The curvature of the conductance band edge inside the dot (the lowest energy allowed for an electron) represents the effect of the spatial confinement energy inside the triangular dot (not to scale). The *horizontal lines* inside the dot indicate the shell structure of the density of states caused by confinement. The Fermi distribution functions in the source (S) and drain (D) reservoirs are indicated by *shading*. **a** In linear response the transmission probability (the conductance) is independent of the absolute value and the sign of the voltage. **b**,**c** The non-linear response regime where the potential and the electron states depend on the applied voltage. When the potential is not inversion symmetric, the electrical current flows via different sets of electronic states for positive and negative voltage, and rectification (that is, a ratchet effect) is observed

Electron billiards in which quantum conductance fluctuations are observed are often referred to as "open quantum dots" [17], because the origin of the fluctuations are the quasi-0D electron states forming inside small electron cavities. Conductance fluctuations in quantum dots can also be observed as a function of any other parameter that is suitable to modify the electron states inside the cavity. Examples are modifications of the cavity shape or a change in the Fermi energy. Experimentally this is done using so-called gates, that is, metal electrodes near to, or on top of, the cavity that can be used to influence the electrons inside the cavity electro-statically [18].

2.2 *Quantum-dot ratchets*

How can we use quantum dots to realize a rocking ratchet? To answer this question, one needs to identify mechanisms by which electron interference in quantum dots induce a non-linear current–voltage dependence. Consider first the limit of small voltages (linear response). Figure 4a shows schematically the bottom of the conduction band (the lowest allowed electron energy) along the symmetry axis of a triangular quantum dot. The variation of the band represents the confinement energy in the point contacts and inside the dot. The bias voltage is assumed to be negligible, such that there is no potential drop between the chemical potentials (visible as the maximum occupied energies) in the source and drain reservoirs. At very small voltages ($|eV| \ll \mu_F, kT$), transport through the dot is via the electron states within a few kT of the Fermi energy [5]. In this regime, (1) can be written as $I = GV$, where $G = 2e^2/hM(\mu_F)t(\mu_F)$ does not depend on voltage and μ_F is the equilibrium Fermi energy. The electron states inside the dot contributing to the current are those at the Fermi energy and are the same for both current directions, such that conductance is symmetric.

The quantum-dot band structure for finite voltage is shown in Fig. 4b,c. The potential drop between the reservoirs distorts the 2D dot potential, U, and therefore changes the exact configuration of electron states inside the dot [8, 19]. Because of the asymmetry, the distortion depends, in general, on the sign of the voltage ($U(V) \neq U(-V)$), such that different sets of electron states inside the dot carry the current depending on the current direction. As a result, $t(\varepsilon, U(V))$ depends on the sign of the voltage, causing non-linear and non-symmetric behavior of the conductance (1). As a second effect, a finite bias voltage increases the width of the Fermi window, $[f_S(\varepsilon) - f_D(\varepsilon)]$, which describes the energy range over which electrons contribute to the conductance. The exact position of this window relative to the conductance band bottom inside the dot depends on how the voltage drop is distributed over the device [20]. When the two point contacts are different, as is necessarily the case for a triangular quantum dot, a different range of quantized electron states will contribute to the current for the two signs of the voltage [7, 19].

Experimental data for the differential conductance, $\partial I(V)/\partial V$, are shown in Fig. 5. In the experiment, a dc bias voltage, V, was added to a small ac voltage (frequency 10–100 Hz), and the differential resistance was measured as a function of V using standard phase-locking techniques. The data shown in Fig. 5 were recorded at a series of different magnetic fields, ranging from zero to about ±18 mT (Fig. 5a and b, respectively), in steps of 2 mT. The sign of the magnetic field refers to the direction of the field. Three important observations should be made here. Firstly, the conductance clearly

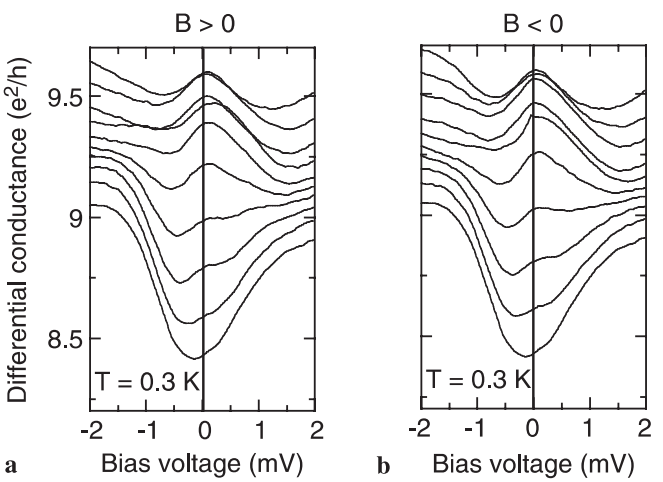

FIGURE 5 Experimental data for the differential conductance, $\partial I(V)/\partial V$, of a triangular electron cavity (Fig. 2a) at increasing perpendicular **a** positive and **b** negative (reversed) magnetic field and a temperature of 0.3 K. The field values *from bottom to top* are for **a** $B = -0.2, +1.8, +3.8, \ldots, +17.8$ mT and for **b** $B = -0.2, -2.2, -4.2, \ldots, -18.2$ mT (note the offset −0.2 mT of the magnetic field values, which is due to a residual field in the magnet). Each curve has been offset by $+0.1e^2/h$ from the preceding one. (From [19])

depends on bias voltage (non-linear response) in a way that is, in general, not symmetric with zero bias voltage – that is, rectification is observed. A more detailed analysis shows that most of the asymmetric behavior is suppressed at temperatures above 1 K, indicating that quantum interference effects are important [19]. Secondly, the non-linear effects change rapidly with magnetic field. Importantly, the magnetic field scale of these changes (a few mT and less) is the same as that of magneto-conductance fluctuations. This scale is thus consistent with magnetic-field-induced modifications to quantum interference (see Sect. 2.1) but not with classical effects (field scale 10–100 mT, see Fig. 3). We can therefore conclude that we observe rectifying behavior related to the voltage-induced modification of transport through electron quantum states inside the dot.

A third important observation to be made from Fig. 5 is related to the symmetry in magnetic field, which allows us to perform an important test: Is the origin of rectification in our device indeed the geometry of the dot and not, for instance, broken symmetry because of random impurities of the material? (Rectification due to impurities in mesoscopic devices has been observed previously, see [21].) If the answer is "yes", then the conductance in the non-linear regime should be symmetric with respect to zero magnetic field, because a horizontal symmetry axis should be present. To understand this, consider that in the linear response regime conduction is always symmetric with respect to zero magnetic field – that is, the relationship $G(B) = G(-B)$ is valid independent of the potential symmetry [5, 22]. In the non-linear regime, however, when the conductance depends on the bias voltage, this general symmetry relationship breaks down and symmetry in magnetic field is normally absent. The symmetry is restored only when the potential has a symmetry axis parallel to the current direction. Under this condition, which is fulfilled in our dot geometry, the relationship $G(V, B) = G(V, -B)$ should be valid. The data shown in Fig. 5 confirm that the non-linear quantum conductance does not depend on the direction of the magnetic field, within a field range that fully alters the non-linear conductance fluctuations. It appears, therefore, that any deviations from the intended dot symmetry are not significant within the parameter range covered here ($|B| < 20$ mT, $|V| < 2$ mV) and that rectification is indeed due to the asymmetric device shape.

This relationship between device shape and the *existence* of rectification does not mean, however, that one can precisely predict the *direction* of rectification of a given device. The reason is that electron-wave interference is extremely sensitive to variations of the Fermi energy and to the exact distribution of charges forming the electrostatic potential, which both depend on the cooling process. While this means that the sign of rectification for a specific set of parameters is not controllable in the device design, it is very easy in an experiment to adjust the direction of rectification, once it is established. One can control the current direction by varying the electron states inside the dot using any of the following experimental variables: the device shape (using an external gate), the Fermi energy (using a top-gate, see Fig. 6) or a small magnetic field (Fig. 5). In addition, the amplitude of the applied ac voltage can be used to reverse the current direction (Fig. 6).

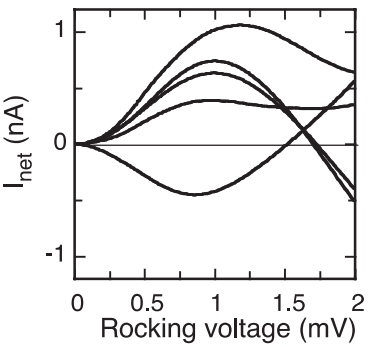

FIGURE 6 The net current generated in a quantum dot ratchet by an ac rocking voltage for different carrier concentrations (Fermi energies) in the 2DEG. The Fermi energy is controlled by applying a voltage to metal layer deposited on top of the electron cavity (a "top gate"). Note that the net current direction can be tuned by varying the Fermi energy or the rocking amplitude

3 Tunneling ratchets

In this section we review a ratchet experiment that makes use of tunneling through an asymmetric energy barrier. The key observation is a ratchet current direction that depends on temperature. We will first describe the experiment (Sect. 3.1) and then provide a model accounting for a temperature-induced current reversal (Sect. 3.2). We will then discuss some differences between the experiment and our model, on the one hand, and the seminal theory on quantum ratchets by Reimann et al. [2], on the other (Sect. 3.3).

3.1 *Experiment*

Figure 7 shows a top-view scanning electron micrograph of a tunneling ratchet for electrons. Etched trenches, visible as darker lines in the image, electrostatically deplete the 2DEG situated about 100 nm underneath the device surface, confining the electrons to a narrow channel with asymmetric, funnel-like constrictions. The lithographic width of this channel has been chosen to be about 100 nm at the narrowest points, corresponding to just a few electron Fermi wavelengths ($\lambda_F \approx 40$ nm). The channel therefore effectively forms a 1D electron wave guide. Because of the lateral confinement energy, an electron moving along the channel experiences each of the periodic constrictions as an asymmetric energy barrier. One can vary the width of the channel (and thus the height of the energy barriers) by charging the electron sheet regions parallel to the channel, using these regions as

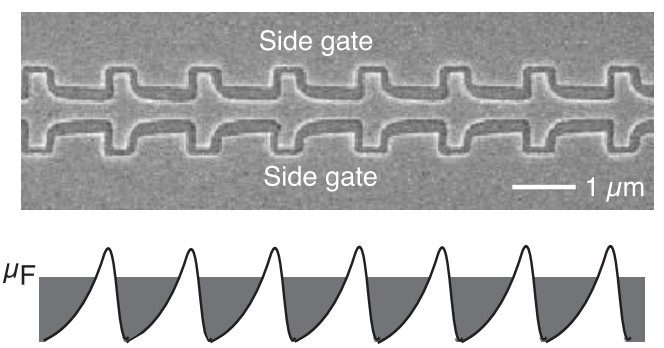

FIGURE 7 An electron tunneling ratchet. *Top*: Scanning electron micrograph; *darker areas* are etched trenches patterned by electron beam lithography and shallow wet etching. By electrically interrupting a two-dimensional electron sheet located below the device surface, they form an electron-wave guide. *Bottom*: Ratchet potential experienced by 1D electrons moving along the wave guide

side-gates. Figure 7 shows the energy variation of the conductance band bottom (the lowest 1D wave mode) along the channel when the narrowest parts of the channel are only about $\lambda_F/2$ wide, such that the confinement energy at these points is of the order of the Fermi energy. Transport in the channel is then possible only by thermal excitation over the energy barriers, or by tunneling through the barriers. The lateral dimensions of each ratchet cell ($\approx 1\,\mu$m) were much smaller than the length scales for elastic (6 μm) and inelastic ($> 10\,\mu$m) scattering at the temperatures and voltages used here (energies kT and $|eV| \leq 1$ meV).

Contact pads (not visible in Fig. 7) situated far away to the left and right of the channel provide electrical access to the 2DEG. Using these contacts as source and drain contacts, a voltage can be applied along the channel. The resulting current, I, is determined by the barriers's reflection and tunneling coefficients and is sensitive to the precise shape of these barriers. Because of the geometric asymmetry, the electric field along the channel produced by the voltage, V, deforms the barriers in a way that depends on the polarity of V, such that $I(V) \neq -I(-V)$. In order to "rock" the ratchet we here used a square-wave source–drain voltage of amplitude V_0. The frequency of the order of 100 Hz was chosen to be much slower than all electronic time scales, such as energy relaxation times (adiabatic rocking). The electronic system was therefore in a steady state at all times, and to understand the ratchet behavior it is sufficient to analyze the two dc situations V_0 and $-V_0$. Transient behavior can be neglected and the time-averaged, net current induced by the rocking is given by $I_{\text{net}} = 0.5\,[I(V_0) + I(-V_0)]$.

As will become clear in the next section, a temperature dependence of the current direction in a tunneling ratchet is detectable when electrons at energies just above and below the top of the barriers contribute to the current. To achieve this condition in the experiment, the barrier height was set to approximately match the Fermi energy, $\mu_F = 11.8$ meV (the relative position of barrier height and Fermi energy can be estimated from the conductance of the point contact – see Eq. (1)). Further, the rocking voltage, V, is chosen such that, by varying T, the width of the Fermi window, about $(|eV| + 4kT)$, can be varied over the energy range around the barrier top where quantum corrections to the transmission probability are important. Calculations show that this energy range extends about 1 meV above and below the barrier maximum. In practice, one chooses a suitable rocking voltage and sweeps the barrier height (using the side gates) at various temperatures [8]. In this way, one finds sets of values for the rocking voltage and the side-gate voltage, where the net current direction depends on temperature. This reversal can then be observed directly by sweeping the temperature, while all other parameters, including the shape and height of the potential barriers, are kept constant. The data shown in Fig. 8a were obtained using a rocking voltage, $V_0 = 1$ mV, corresponding to a voltage drop of 0.1 mV over each barrier (less than 1% of μ_F) in the device shown in Fig. 7, which consisted of 10 ratchet barriers in total. The net current generated in this way corresponds to about 1 to 5% rectification of the total current and, at 4 K, was initially positive but reversed its direction as the temperature was reduced to 0.4 K.

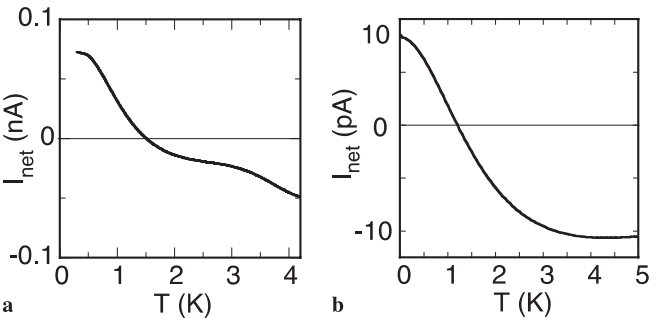

FIGURE 8 **a** Measured net electric current, induced by "rocking" the ratchet potential in Fig. 7 by a square-wave voltage of amplitude 1 mV, versus temperature. (Data from [8]. Note that positive electrical current corresponds to a *particle current* from right to left [12]). **b** Calculated data of the net current for a rocking voltage of amplitude 0.5 mV and Fermi energy 11.7 meV (see Sect. 3.2 for details of the model used)

To detect any contribution to I_{net} not related to the asymmetry of the device, each experimental sweep was carried out in the forward and reverse configurations of the device (the source and drain leads were physically interchanged using a switch). If care is taken to ensure that no significantly nonlinear elements are in the path of the measurement current, and that the sum of Ohmic resistances (such as leads, ballast resistors and contacts pads) on either side of the device are balanced, then rectifying effects that are not due to the asymmetry of the device, such as self-gating [23], can be removed by adding the two data sets [24].

3.2 *Model*

The observed reversal of the current direction as a function of temperature can be explained intuitively by considering how the shape of the energy barriers deforms in an electric field and how this change affects electron transmission. In Fig. 9 we show estimated barrier shapes for the device in Fig. 7 for negative (Fig. 9a) and positive (Fig. 9b) bias voltage applied to the left reservoir [12]. In each case,

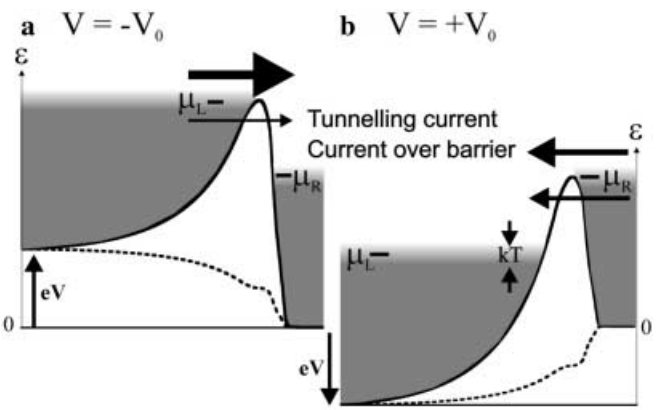

FIGURE 9 Model of a single ratchet barrier of the device in Fig. 7. The shape of the barrier is based on the lithographic shape of the electron wave guide and has a maximum barrier height of 12 meV at zero bias. To obtain the barrier at finite **a** negative or **b** positive voltage, an assumption for the spatial distribution of the voltage drop needs to be made (*dashed line*). The *arrows* indicate the flow directions of electrons (electron flow from right to left corresponds to positive electrical current [12])

the flow of electrons is "downhill", as indicated by the arrows. Crucially, however, when the barrier is tilted to the right ($V < 0$), it deforms to be thicker at a given energy under the barrier top than when tilted to the left ($V > 0$). Consequently, the energy composition of the current is different for $V > 0$ and $V < 0$: a thicker barrier reduces the probability for tunneling through the barrier, but, at the same time, makes it easier for electrons with high energy to cross over the barrier, because the smoother shape reduces wave reflection. Smoothness of the barrier is important because our ratchet is essentially a 1D wave guide, and any rapid spatial change of the potential leads to partial wave reflection even when the electron has enough energy to pass above the barrier. The electron flow above the barrier is thus larger for $V < 0$ than for $V > 0$, while the flow of electrons that tunnel through the barrier is larger for $V > 0$ than for $V < 0$. Averaged over a full period of symmetric rocking, there is a net particle current to the left consisting of electrons with low energy that tunnel through the barriers. At higher energy, a net current flows to the right, consisting of electrons that pass over the top of the barrier. The direction of the total, energy-averaged net current, I_{net}, depends then on the electron energy distribution. At high temperatures, the current to the left (negative electrical current) will usually dominate, because electrons of higher energy are available. As the temperature decreases, however, this contribution can become smaller than the tunneling current, and a reversal of the total net current can be observed.

To quantitatively model the net current as a function of temperature, we assume that transport across each energy barrier is ballistic and that no inelastic processes occur (that is, the electrons do not change their energy while traversing the barrier), and we consider electron transport in the lowest 1D wave mode only ($M = 1$ in (1)), assuming that any higher 1D wave modes are not populated at the narrowest points of the wave guide. The electric current driven by a bias voltage, V, applied between the 2DEG reservoirs at either end of the channel is [5]

$$I(V) = \frac{2e}{h} \int_0^\infty t(\varepsilon, V)\,[f_{\mathrm{L}}(\varepsilon, V) - f_{\mathrm{R}}(\varepsilon, V)]\,\mathrm{d}\varepsilon\,. \qquad (2)$$

Here, $f_{\mathrm{L/R}}(\varepsilon, T) = 1/\left(1+\exp\left[(\varepsilon-\mu_{\mathrm{L/R}})/kT\right]\right)$ are the Fermi distribution functions in the electron reservoirs to the left (L) and right (R) of the barrier. $t(\varepsilon, V)$ is the probability that electrons are transmitted through the device. We assume that $(|eV|, kT) \ll \mu_{\mathrm{L/R}}$, which allows us to use zero as the lower limit of integration, independent of the voltage sign.

To find the current at a given bias voltage, we need to calculate the transmission function, $t(\varepsilon)$, of the barrier at that voltage. The form of the energy barriers at zero bias voltage can be estimated from the lithographic shape of the channel and the lateral electron confinement energy (Fig. 7; for details see [8]). To obtain the barrier shape at finite voltage, the spatial distribution of the potential drop between reservoirs needs to be known, which self-consistently depends on screening effects. Here we assume a spatial distribution of the voltage drop that is proportional to the local derivative of the barrier (Fig. 9). This model is based on the notion that a more rapid potential variation leads to stronger wave reflection, and therefore a more rapid local voltage drop [20]. This particular choice has the side effect that the barrier height changes with voltage in a symmetric manner, resulting in the suppression of a classical contribution to the net current. We will come back to this point in Sect. 3.3.

Once the barrier shapes at $V > 0$ and $V < 0$ are known, the transmission $t(\varepsilon)$ is calculated for each of the two voltages by solving the 1D Schrödinger equation (see inset to Fig. 10), and the dc current for each voltage can be calculated using (2). The (time-averaged) net current induced by a square-wave voltage switching between $\pm V_0$ can be written as follows [8]:

$$I_{\mathrm{net}}(V_0) = \frac{e}{h} \int_0^\infty \Delta t(\varepsilon, V_0)\,\Delta f(\varepsilon, V_0)\,\mathrm{d}\varepsilon\,, \qquad (3)$$

where $\Delta f(\varepsilon, V_0) \equiv [f_{\mathrm{L}}(\varepsilon, V_0) - f_{\mathrm{R}}(\varepsilon, V_0)]$ is the "Fermi window", the range of electron energies which contribute to the current. The term $\Delta t(\varepsilon, V_0) \equiv [t(\varepsilon, V_0) - t(\varepsilon, -V_0)]$ is the difference between the transmission probabilities for positive and negative voltages and is shown in Fig. 10. For $V_0 = 0.5\,\mathrm{mV}$, we find that $\Delta t(\varepsilon)$ is of the order of 10^{-3}, for energies within a few meV of the barrier height used in the model, $E = 12.0\,\mathrm{meV}$ (Fig. 10). The energy window $\Delta f(\varepsilon)$ is shown in Fig. 10 for $V_0 = 0.5\,\mathrm{mV}$, $\mu_{\mathrm{F}} = 11.7\,\mathrm{meV}$ and three different temperatures. Electrons with energies smaller than the barrier height are more likely to tunnel from right to left ($V = V_0$) when the barrier becomes thinner than from left to right ($V = -V_0$) when the barrier

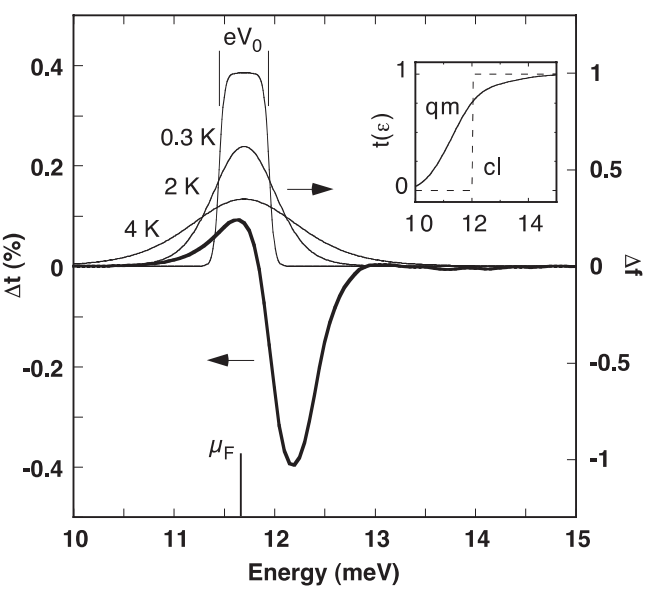

FIGURE 10 The *bold line* is $\Delta t(\varepsilon)$, the difference between the transmission functions for positive and negative bias voltage for the potential barrier in Fig. 9. *Thin lines* are the Fermi windows, $\Delta f(\varepsilon)$, that is, the range of electron energies contributing to the current for the temperatures indicated (see text for further details). The net current is given by the integrated product $\Delta t(\varepsilon)\Delta f(\varepsilon)$ (see (3)). At $T = 0.3$ K the electron flow within Δf samples an area where Δt is negative. At 4 K, Δf samples an energy range where Δt is predominantly positive, and the current reverses direction. The *inset* shows the classical and quantum mechanical transmission functions, $t(\varepsilon)$, for a barrier height of 12 meV. Quantum-mechanical corrections extend about 1 meV above and below the barrier maximum

becomes thicker. This results in Δt being positive in this energy range. For energies above the barrier height the situation is reversed: electron wave reflection is stronger for steep, thin barriers (for $V = V_0$) than for the smoother, thicker barrier ($V = -V_0$), and Δt is negative in that energy range. As Δf is adjusted (through changing T, V_0 or the Fermi energy) to sample the Δt curve where it is negative rather than positive, the net current reverses direction.

3.3 *Discussion: three ways of producing a current in an adiabatic tunneling ratchet*

So far in our discussion of a rocking tunneling ratchet we have concentrated on the quantum-mechanical contributions to the net current. It is important to note, however, that a classical contribution is also possible. Consider the energy barriers used in our model as shown again in Fig. 11a. To obtain the shape of the barrier under tilt we used a "best-guess" spatial distribution of the voltage drop that scales with the local gradient of the barrier at $V = 0$. The physical reasons for this assumption are wave-mechanical considerations: a voltage drop occurs when electrons are reflected, and a fast variation of the potential leads to more wave reflection than a smooth variation. As a side effect of this model, exactly half of the voltage drop occurs on either side of the barrier maximum, such that the barrier height is independent of the voltage sign. Because the classical transmission probability depends only on the barrier height, no classical net current is possible, and all net current observed in this model is of quantum-mechanical origin.

For comparison, in Fig. 11b we show the potential and tilt used in the seminal work on quantum ratchets by Reimann et al. [2]. These authors used a linear tilt which leads to a lower effective barrier for tilt to the right than for tilt to the left, because the portions of the potential drop occurring before and after the barrier maximum are different. In this case, a classical contribution to the net current is observed: the current due to thermal excitation is stronger for tilt to the right, where the effective barrier height is lower, than for tilt to the left.

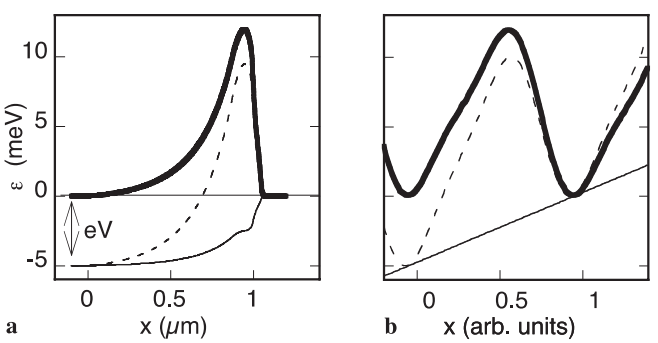

FIGURE 11 Comparison of the ratchet potential used in the model of Sect. 3.2 and in the work by Reimann et al. [2]. **a** In the present work, the ratchet barrier at zero bias voltage (*bold line*) is derived from the lithographic shape of the wave guide. To obtain the barrier shape at a finite voltage (*dashed line*), a spatially varying potential gradient (*thin line*) is added. This particular shape of the potential drop results in the same barrier height for positive and negative applied voltage. The classical net current is therefore zero for adiabatic rocking. **b** In the model by Reimann et al. [2] a linear tilt was assumed, which results in a lower barrier for one tilt direction, because the portions of the potential drop before and after the barrier maximum are different. A classical contribution to the ratchet current is then possible

In the general case one needs to consider three contributions to the net current in adiabatic rocking ratchets: (i) a classical current flowing in the direction of the shallower slopes (to the right in Fig. 11) due to changes in the barrier *height*; (ii) a tunneling current in direction of the steeper slopes (to the left) due to the barrier *shape*; and (iii) a wave-mechanical contribution flowing in the direction of the shallower slopes (to the right) which also is related to the barrier *shape*. Contributions (i) and (iii) flow at high energies and in a direction opposite to the tunneling current flowing at low energies (ii). Our own model (Sect. 3.2) considered only components (ii) and (iii). The model in [2], on the other hand, considered components (i) and (ii). In general, all three contributions can be of importance. In particular, it can be expected that a full self-consistent analysis of the barrier shape in our experimental device will yield a finite dependence of the barrier height on voltage direction, which would lead to a finite classical ratchet current in addition to the quantum-mechanical current contributions considered in Sect. 3.2.

The fact that the current reversal as a function of temperature is observed in both models illustrated in Fig. 11, in spite of their differences, underlines that this effect can be viewed as a general signature of adiabatic tunneling ratchets [25]. Another signature observed in both models is a finite net current in the limit of very low temperatures: while in classical ratchets the current due to thermal excitation goes to zero for $T \to 0$, both models in Fig. 11 yield a finite quantum net current when T approaches zero (see also Fig. 8).

4 Quantum heat pumps

The analysis of ratchets usually concentrates on the particle flow. In the present section we discuss how ratchets for which the direction of the particle current depends on temperature can also be interpreted as heat pumps [9]. This is easiest to see by considering the situation in which the net particle flow due to tunneling, flowing at low energies, is exactly counter-balanced by the thermally excited net current flowing at higher energies (Fig. 9). In this situation, where the net particle flow is zero, the ratchet clearly pumps heat. In the more general case, when the net particle flow is finite, the heat flow due to the ratchet's heat pumping action is superimposed on the net energy current that trivially accompanies any finite particle current. For clarity, the following analysis will assume a situation where the net particle current is zero (that is, $I_{\mathrm{net}} = 0$ in (3)).

To derive the heat current accompanying the net charge current, we note that the heat added when one electron is transferred to a reservoir with chemical potential μ is given by $\Delta Q = (\Delta U - \mu)$, where ΔU is the change in internal energy associated with the addition of the electron. We consider again the single ratchet barrier of Fig. 9, connecting two 2D electron reservoirs, R and L. The change in heat in R and L, respectively, upon transfer of one electron from the left to the right is given by $\Delta Q_{\mathrm{R/L}} = \pm(\varepsilon - \mu_{\mathrm{R/L}})$. By replacing the electron charge, e, by a factor of $\Delta Q_{\mathrm{R/L}}$ inside the integral of (2), the steady heat current at a given bias voltage, V, can be written

as follows:

$$q_{\mathrm{R/L}} = \pm\frac{2}{h}\int_0^\infty (\varepsilon - \mu_{\mathrm{R/L}})t(\varepsilon, V)\Delta f(\varepsilon, V)\,\mathrm{d}\varepsilon\,. \tag{4}$$

Note that $q_{\mathrm{R}}(V)$ (the heat current entering R) exceeds $-q_{\mathrm{L}}(V)$ (the heat current leaving L) by the externally supplied Joule heating power, IV. The net (time-averaged) heat current into the right and left reservoirs is [9]

$$q^{\mathrm{net}}_{\mathrm{R/L}}(V_0) = 0.5\left[q_{\mathrm{R/L}}(V_0) + q_{\mathrm{R/L}}(-V_0)\right].$$

It is illustrative to write this equation in the following form:

$$\begin{aligned} q^{\mathrm{net}}_{\mathrm{R/L}} &= \frac{1}{2}\left[q^{\mathrm{net}}_{\mathrm{R}} + q^{\mathrm{net}}_{\mathrm{L}}\right] \pm \frac{1}{2}\left[q^{\mathrm{net}}_{\mathrm{R}} - q^{\mathrm{net}}_{\mathrm{L}}\right] \\ &= \frac{1}{2}\Omega \pm \frac{1}{2}\Delta E \\ &= \frac{eV_0}{h}\int_0^\infty \tau\Delta f\,\mathrm{d}\varepsilon \pm \frac{1}{h}\int_0^\infty \left(\varepsilon - \frac{\mu_{\mathrm{R}} + \mu_{\mathrm{L}}}{2}\right)\Delta t\Delta f\,\mathrm{d}\varepsilon\,. \end{aligned} \tag{5}$$

Here the upper and lower symbol in $\pm$ refers to R and L, respectively. The last line of (5) is obtained by writing the chemical potentials in the form $\mu_{\mathrm{R/L}} = [(\mu_{\mathrm{R}} + \mu_{\mathrm{L}})/2 \pm eV_0/2]$, and $\tau(\varepsilon, V_0) = 0.5\,[t(\varepsilon, +V_0) + t(\varepsilon, -V_0)]$ is the average transmission probability for $V = V_0$ and $V = -V_0$.

One can interpret (5) as follows: $\Omega = q^{\mathrm{net}}_{\mathrm{L}} + q^{\mathrm{net}}_{\mathrm{R}}$ is the electrical power input (Joule heating), averaged over one cycle of rocking. Ω is essentially the "waste heat" generated by operating the ratchet as a heat pump, and is proportional to the average electron current flow. $\Delta E = q^{\mathrm{net}}_{\mathrm{R}} - q^{\mathrm{net}}_{\mathrm{L}}$ is the heat pumped from the left to the right sides of the device due to the energy-sorting properties of the ratchet. ΔE can be finite only when $\Delta t \neq 0$, that is, for asymmetric, ratchet barriers. In a sense the ratchet acts as a badly constructed refrigerator because it pumps heat from one reservoir to another, but deposits waste heat in both reservoirs. The performance of the ratchet as a heat pump can be quantified by a coefficient of performance, $\chi = |\Delta E|/\Omega$. When $\chi < 1$, both reservoirs are heated ($\Omega > |\Delta E|$), but one more than the other. Cooling of one reservoir takes place when $\chi > 1$.

A numerical analysis of the experimental device shown in Fig. 7 yields values for χ on the order of 1% [9]. This low efficiency is a result of the fact that the potential barrier of Fig. 9 transmits electrons in a wide range of energies in both rocking directions (all of which contribute to heating), while the ratio $\Delta t/\tau$ is less than 1%. Using sharp energy filters, such as resonant tunneling barriers [26], potentials where $\Delta t/\tau \cong 1$ can be realized in principle. Cooling of one reservoir, that is, $\chi > 1$, can then be achieved, which opens interesting avenues to mesoscopic heat pumps. Such a heat pump can then also be operated in reverse, using the difference in temperature between two electron reservoirs to generate electrical energy [10]. A fundamental question is whether the ideal Carnot efficiency of a heat engine can be obtained in such a system. Recent results show that this is indeed the case: a heat engine based on a ratchet device can, in principle, operate arbitrarily close to the Carnot efficiency when ideal energy filters are used and when the energy at which the filters transmit are chosen appropriately [10].

5 Outlook

The experimental exploration of quantum ratchets is still in its very early stages. The two experiments reviewed here belong to the group of adiabatic rocked ratchets. In a way this is the regime that is most easily accessible to intuitive understanding. The condition of adiabatic (slow) changes of the potential tilt means that the system is in a steady state at each instant, and transient behavior can be neglected. In our experimental regime electrons are "moderately damped" – they have an inelastic scattering length comparable to the size of one ratchet cell. In this regime one can neglect inelastic processes while an electron passes a barrier, but one can also assume that it will soon afterwards become part of the thermal distribution. This simplifies the analysis of a rocking ratchet enormously, because it is sufficient to analyse a single barrier. The periodicity of the ratchet device shown in Fig. 7 adds no new physics.

The theory community has already explored beyond this regime, considering non-adiabatic systems [27], fluctuating potentials [28] and semi-classical systems [29] (for an overview, see [25]). Future experimental work should address the so-called non-adiabatic regime, in which the potential is rocked at a frequency comparable to characteristic times of the particles, such as their escape time through ratchet barriers or the rate of energy dissipation. For moderately damped classical particles in ratchets rocked on time scales comparable to the "time of flight" of a particle along one ratchet period, chaotic behavior of the current direction is predicted [30]. Chaos in quantum ratchets may give rise to novel signatures of quantum chaos in non-equilibrium systems [31]. An experimental realization of fast potential changes would allow the construction of so-called flashing ratchets, where the potential itself is modified and no external forces are applied at any time. Semiconductor devices will remain a promising environment for experiments of new quantum-ratchet systems, including semi-classical ratchets [29], ratchets in which quantum chaos may lead to new effects [31], and periodic ratchets small enough to allow the formation of mini-bands [32]. Other promising experimental systems for the study of quantum-ratchet effects include optical ratchets for ultracold atoms [33] and ratchets for vortices in superconductors [34].

ACKNOWLEDGEMENTS This research was supported by the Australian Research Council, by the Swedish Research Councils for Engineering and Natural Sciences, and by the Swedish Foundation of Strategic Research. Writing of this review was supported by the University of Oregon.

REFERENCES

1 P. Reimann, P. Hänggi: Appl. Phys. A, **75**, 235 (2002), DOI 10.1007/s003390201331
2 P. Reimann, M. Grifoni, P. Hänggi: Phys. Rev. Lett. **79**, 10 (1997)
3 M.O. Magnasco: Phys. Rev. Lett. **71**, 1477 (1993); A. Ajdari: J. Phys. I (Paris) **4**, 1577 (1994); P. Hänggi, R. Bartussek: In *Nonlinear Physics of Complex Systems – Current Status and Future Trends*, ed. by J. Parisi, S.C. Müller, W. Zimmermann (Springer, Berlin 1996)

4 C.W.J. Beenakker, H. van Houten: In *Solid State Physics*, ed. by H. Ehrenreich, D. Turnbull (Academic Press, Boston, 1991), Vol. 44
5 S. Datta: *Electronic Transport in Mesoscopic Systems* (Cambridge University Press, Cambridge, 1995)
6 R. Landauer: In *Nonlinearity in Condensed Matter*, ed. by A.R. Bishop, D.K. Campbell, P. Kumar, S.E. Trullinger (Springer Verlag, Berlin 1987)
7 H. Linke, P. Omling, H. Xu, P.E. Lindelof: In Proc. 23rd Int. Conf. on the Phys. of Semicond., ed. by M. Scheffler, R. Zimmermann (World Scientific, Singapore, 1996), p. 1593; H. Linke, W. Sheng, A. Löfgren, H. Xu, P. Omling, P.E. Lindelof: Europhys. Lett. **44**, 341 (1998)
8 H. Linke, T.E. Humphrey, A. Löfgren, A.O. Sushkov, R. Newbury, R.P. Taylor, P. Omling: Science **286**, 2314 (1999)
9 T.E. Humphrey, H. Linke, R. Newbury: Physica E **11/2–3**, 281 (2001)
10 T.E. Humphrey, R. Newbury, R.P. Taylor, H. Linke: cond-mat/0201087, (2002)
11 R. Landauer: Philos. Mag. **21**, 863 (1970)
12 Throughout this paper we follow the sign convention used, for instance, in the book by Datta [5]. The electronic charge is $e = -1.6 \times 10^{-19}$ C. A positive voltage applied to the source (the left reservoir) induces a positive electrical current flowing from source to drain (from left to right). This electrical current is generated by an electron *particle* current flowing in the opposite direction, from right to left.
13 H. Linke, L. Christensson, P. Omling, P.E. Lindelof: Phys. Rev. B **56**, 1440 (1997)
14 L. Christensson, H. Linke, P. Omling, P.E. Lindelof, K.-F. Berggren, I.V. Zozoulenko: Phys. Rev. B **57**, 12 306 (1998)
15 S.M. Reimann, M. Persson, P.E. Lindelof, M. Brack: Z. Phys. B **101**, 377 (1996); M. Brack, R.K. Badhuri: *Semiclassical Physics* (Addison-Wesley, 1997)
16 J.P. Bird, D.K. Ferry, R. Akis, Y. Ochiai, K. Ishibashi, Y. Aoyagi, T. Sugano: Europhys. Lett. **35**, 529 (1996); M. Persson, J. Pettersson, B. v. Sydow, P.E. Lindelof, A. Kristensen, K.F. Berggren: Phys. Rev. B **52**, 8921 (1995)
17 J. Bird: J. Phys. C **11**, R413 (1999)
18 R.P. Taylor: Nanotech. **5**, 183 (1994)
19 H. Linke, W. Sheng, A. Svensson, A. Löfgren, L. Christensson, H. Xu, P. Omling: Phys. Rev. B **61**, 15 914 (2000)
20 H. Xu: Phys. Rev. B **47**, 15 630 (1993)
21 S.B. Kaplan: Surf. Sci. **196**, 93 (1988); R.A. Webb, S. Washburn, C.P. Umbach: Phys. Rev. B **37**, 8455 (1988); P.A.M. Holweg, J.A. Kokkedee, J. Caro, A.H. Verbruggen, S. Radelaar, A.G.M. Jansen, P. Wyder: Phys. Rev. Lett. **67**, 2549 (1991); D.C. Ralph, K.S. Ralls, R.A. Buhrmann: Phys. Rev. Lett. **70**, 986 (1993); R. Taboryski, A.K. Geim, M. Persson, P.E. Lindelof: Phys. Rev. B **49**, 7813 (1994)
22 M. Büttiker: IBM J. Res. Developm. **32**, 317 (1988)
23 N.K. Patel, J.T. Nicholls, L. Martin-Moreno, M. Pepper, J.E.F. Frost, D.A. Ritchie, G.A.C. Jones: Phys. Rev. B **44**, 13 549 (1991); A. Kristensen, H. Bruus, A.E. Hansen, J.B. Jensen, P.E. Lindelof, C. Marckmann, J. Nygård, C.B. Sorensen, F. Beuscher, A. Forchel, M. Michel: Phys. Rev. B **62**, 10 950 (2000)
24 T.E. Humphrey, A. Löfgren, H. Linke: unpublished (2002)
25 P. Reimann: Phys. Rep. **361**, 57 (2002)
26 H.L. Edwards, Q. Niu, A.L. de Lozanne: Appl. Phys. Lett. **63**, 1815 (1993); H.L. Edwards, Q. Niu, G.A. Georgakis, A.L. de Lozanne: Phys. Rev. B **52**, 5714 (1995)
27 I. Goychuk, M. Grifoni, P. Hänggi: Phys. Rev. Lett. **81**, 649 (1998); I. Goychuk, P. Hänggi: Europhys. Lett. **43**, 503 (1998)
28 S. Yukawa, M. Kikuchi, G. Tatara, H. Matsukawa: J. Phys. Soc. Jpn. **66**, 2953 (1997)
29 H. Schanz, M.-F. Otto, R. Ketzmerick, T. Dittrich: Phys. Rev. Lett. 87, 070 601 (2001)
30 P. Jung, J.G. Kissner, P. Hänggi: Phys. Rev. Lett. **76**, 3436 (1996); J.L. Mateos: Phys. Rev. Lett. **84**, 258 (2000)
31 H. Linke, T.E. Humphrey, R.P. Taylor, R. Newbury: Phys. Scr., T. **90**, 54 (2001)
32 K.N. Alekseev, E.H. Cannon, J.C. Mc Kinney, F.V. Kusmartsev, D.K. Campbell: Phys. Rev. Lett. **80**, 2669 (1998)
33 C. Mennerat-Robilliard, D. Lucas, S. Guibal, J. Tabosa, C. Jurcak, J.-Y. Courtois, G. Grynberg: Phys. Rev. Lett. **82**, 851 (1999)
34 J.E. Mooij: Private communication (1999)